RSC Advances

ROYAL SOCIETY OF CHEMISTRY

PAPER

View Article Online
View Journal | View Issue

Check for updates

Cite this: *RSC Adv.*, 2023, **13**, 20674

Comparative studies of upconversion luminescence and optical temperature sensing in Tm^{3+}/Yb^{3+} codoped $LaVO_4$ and $GdVO_4$ phosphors

Madan M. Upadhyay, Kumar Shwetabh and Kaushal Kumar *

Received 17th May 2023
Accepted 3rd July 2023

DOI: 10.1039/d3ra03273f

rsc.li/rsc-advances

Tm^{3+}/Yb^{3+} codoped $LaVO_4$ and $GdVO_4$ phosphors are successfully synthesized using solid state reaction methods and then upconversion emission studies are performed. X-ray diffraction has confirmed a pure monoclinic phase of $LaVO_4$ and a tetragonal phase of $GdVO_4$. Upconversion emission through 980 nm laser diode excitation has shown a strong blue band at 475 nm and two weak red bands at 647 and 700 nm originating from $^1G_4 \rightarrow {}^3H_6$, $^1G_4 \rightarrow {}^3F_4$ and $^3F_3 \rightarrow {}^3H_6$ transitions of Tm^{3+} ions, respectively. Non-thermally coupled levels *viz.* $^3F_3$ (700 nm) and $^1G_4$ (475 nm) in both the phosphors are used for fluorescence intensity ratio based optical thermometric studies and a comparison is made. The FIR data against temperature were fitted with polynomial and exponential fittings. The results show that polynomial fitting has a higher absolute sensitivity of 21.2×10^{-3} K^{-1} at 653 K for the $LaVO_4$: Tm^{3+}/Yb^{3+} phosphor than the exponential fitting sensitivity of 19.0×10^{-3} K^{-1} at 653 K, while in the case of the $GdVO_4$: Tm^{3+}/Yb^{3+} phosphor both fitting functions provided the same value of absolute sensitivity, that is 13.0×10^{-3} K^{-1} at 653 K. A comparison of the sensitivity values shows that the $LaVO_4$: Tm^{3+}/Yb^{3+} phosphor provides higher sensitivity than the $GdVO_4$: Tm^{3+}/Yb^{3+}phosphor but the latter one is too high in upconversion emission.

1. Introduction

Rare earth doped upconverting phosphors, which convert lower-energy photons to higher-energy photons, have triggered widespread interest in recent decades because of their excellent properties and vast potential applications in solar cells, display devices, light emitting diodes, bio-imaging, optical thermometry *etc.*[1–8] Nevertheless, upconversion (UC) luminescent materials are currently hampered by low emission efficiency which restricts their field applications in several cases. Therefore, it is crucial to find ways to improve their UC efficiency. Several methods for the improvement in upconversion emission efficiency have been proposed so far and the selection of appropriate host, doping of light ions, use of plasmonic particles *etc.*[9–11] are some popular ways for this purpose. For maximum upconversion efficiency a low phonon energy host is generally preferred that decreases nonradiative losses.[12–14] In this aspect, fluoride hosts are found to be good but unfortunately they suffer lower chemical and photo-physical stability than oxides.[14] Hence, researchers are trying to improve the upconversion emission with oxide hosts.

Among various oxide matrices, lanthanide orthovanadates ($LnVO_4$; Ln: La, Gd, Y) are found crucial for doping of rare earth ions due to their distinct optical, chemical, and electronic properties. These lanthanide orthovanadates generally exist in tetragonal (*t*-) zircon type structure. The zircon type yttrium orthovanadate (YVO_4) and gadolinium orthovanadate ($GdVO_4$) have been studied for upconversion emission and strong upconversion luminescence is noted in these hosts.[15,16] The $LaVO_4$ host however, is found to exist in two polymorphs, either tetragonal (*t*-) zircon type structure or monoclinic (*m*-) monazite type structure depending upon the reaction methods.[14] Lanthanide ions with a larger ionic radius prefer to choose monazite structure because of its higher oxygen coordination number (9).[15] On the line of YVO_4 and $GdVO_4$ hosts it is expected that $LaVO_4$ can be a good candidate for strong upconversion emission which is also revealed by Shao *et al.*[17] It is feasible to create multi-colored emission by doping with various rare earth (Ln^{3+}) ions, such as red from Eu^{3+}, green from Er^{3+}, and blue from Tm^{3+} ions. The $LaVO_4$ is substantially less expensive and is based on a resource that is far more abundant than Y. The current objective is to synthesize $LaVO_4$-based phosphor and to compare it with popular $GdVO_4$ host. The thermodynamically stable monazite-type $LaVO_4$ can be prepared *via* conventional solid–state reaction method. However, problem lies in the preparation of zircon type $LaVO_4$ due to its metastable nature. Many researchers have synthesized zircon type $LaVO_4$ through various synthesis methods. For instance, Oka *et al.*[18] have reported the synthesis of high crystalline zircon type tetragonal $LaVO_4$ using hydrothermal

Optical Materials & Bio-imaging Research Laboratory, Department of Physics, Indian Institute of Technology (Indian School of Mines), Dhanbad 826004, India. E-mail: kkumar@iitism.ac.in

method. Similar observation is made by Jia *et al.*, and according to them monazite and zircon phased $LaVO_4$ nanocrystals may be produced hydrothermally and in a controlled manner using additives like EDTA.[19]

Among lanthanide ions the thulium Tm^{3+} ion emits strong upconversion emission spanning from ultravoliate (UV) to near-infrared (NIR) region upon 980 nm excitation. As a result, it is widely used activator ion for upconversion emission. Taking advantage of the efficient energy-transfer from sensitizer and activator, the Yb^{3+} ion as sensitizer is used with Tm^{3+} ion. The energy transfer from Yb^{3+} to other ions is effectively facilitated by the fact that the $^2F_{7/2} \rightarrow {}^2F_{5/2}$ transition of Yb^{3+} is strongly resonant with the f–f transitions of common upconverting lanthanide ions including Er^{3+}, Tm^{3+}, and Ho^{3+}.[20–24] Furthermore, the energy difference between the excited and the ground states of the Yb^{3+} ion is roughly 10 000 cm^{-1}, which corresponds to the low-cost 980 nm laser diode excitation. To the best of our knowledge, the literature does not have any reports on the upconversion and optical thermometric characteristics of either monazite-type or zircon-type $LaVO_4$ codoped with Tm^{3+}/Yb^{3+} ions.

Temperature sensing is crucial in a variety of sectors including research, industrial application, medicine, and others. Traditional temperature detection techniques frequently involve contact measurement and these thermometers often fall short of the demands for their applications in a variety of challenging and harsh environments such as in tissue cells.[25] Therefore, temperature monitoring technique based on fluorescence intensity ratio (FIR) is regarded as promising due to its non-contact, high sensitivity, and broad detection range benefits.[26] Change in FIR with temperature is often caused by repopulation of electrons in thermally coupled levels (TCLs) upon thermal excitation. The energy gap (ΔE) between thermally coupled levels should be in the range 200–2000 cm^{-1}. In principle, a larger energy gap (ΔE) indicates higher sensitivity.[27] Consequently, it is a serious issue to increase sensitivity while taking the smaller (ΔE) between TCLs into account. For example, the energy difference between $^3F_3$ and $^3H_4$ excited energy levels of Tm^{3+} ion is about 1817 cm^{-1}, which is extremely near to the maximum limit range of TCLs. So these levels will give high temperature sensitivity.[28,29] Most of the energy level pairs in rare earth ions are non-thermally coupled levels (NTCLs). In actuality, the luminescence produced by NTCLs is also temperature-dependent since it results from the emission bands of two excited states that behave differently as a function of temperature. As a consequence, the FIR between these states is substantially temperature-dependent. NTCLs-based FIR technique, opposed to TCL-based FIR technique, is not restricted by difference in energy levels and may thus have better temperature sensitivity.[30,31]

Herein, monoclinic $LaVO_4$: Tm^{3+}/Yb^{3+} and tetragonal $GdVO_4$: Tm^{3+}/Yb^{3+} phosphors were synthesized *via* conventional solid–state reaction method for comparison of upconversion emission and non-contact temperature sensitivity in the temperature range 300–653 K under 980 nm laser diode excitation. Non-thermally coupled level $^3F_3$ and $^1G_4$ of Tm^{3+} ion are utilized for temperature sensing application in both the phosphors. Colour tuning is also studied with the help of energy level and CIE chromaticity diagram.

2. Experimental

2.1. Materials

To synthesize Tm^{3+}/Yb^{3+} codoped $LaVO_4$ and $GdVO_4$ phosphors, La_2O_3 (99.99%, Alfa Aesar), Gd_2O_3 (99.99%, Alfa Aesar), V_2O_5 (99.99%, Alfa Aesar), Tm_2O_3 (99.99%, Alfa Aesar), Yb_2O_3 (99.99%, Alfa Aesar) were taken as initial materials.

2.2. Synthesis

Monazite type $LaVO_4$: Tm^{3+}/Yb^{3+} and zircon type $GdVO_4$: Tm^{3+}/Yb^{3+} phosphors were synthesized by high-temperature solid–state reaction technique. For both hosts the concentrations of Tm^{3+} and Yb^{3+} were taken as 0.3 mol% and 5 mol%, respectively based on literature.[28] The calculated amounts of Gd_2O_3, La_2O_3, V_2O_5, Tm_2O_3 and Yb_2O_3 were individually mixed and grinded homogeneously in an agate mortar for 1 h each using acetone as mixing medium. The obtained powder was kept in alumina crucible and then heated at a rate of 5° per min in an electrical furnace set to 1473 K for 8 hours. After cooling to ambient temperature, the materials were crushed to get fine powders for further characterizations.

2.3. Characterizations

Rigaku smartlab X-ray diffractometer with Cu Kα radiation source ($\lambda = 0.15406$ nm) was employed to determine the crystal phases of the produced phosphors. Agilent Cary 5000 UV-vis-NIR spectrophotometer in 200–1200 nm wavelength range was utilized to record the absorption spectra of the synthesized samples. A CCD-based spectrometer (Avantes, ULS2048 × 64) was used to record upconversion emission spectra of the prepared samples using 980 nm laser diode as the excitation source. A self-fabricated heating element was used to measure the temperature-dependent upconversion spectra in the temperature range of 300–653 K. To avoid the laser-induced optical heating of the material, the laser power was maintained at 66 mW. All the measurements were performed using the materials in powder form at room temperature.

3. Results and discussion

3.1. X-ray diffraction (XRD) analysis

The XRD analysis was carried out to ascertain the phase identity and purity of both the prepared samples and recorded patterns are shown in Fig. 1(a and b). Fig. 1(a) shows the XRD pattern of the $LaVO_4$: Tm^{3+}/Yb^{3+} while Fig. 1(b) represents XRD pattern of $GdVO_4$: Tm^{3+}/Yb^{3+} phosphor. The diffraction peaks were well matched with the typical monoclinic phase of $LaVO_4$ (JCPDS No: 01-070-2392) with the space group $P2_1/n$ (14) and tetragonal phase of $GdVO_4$ (JCPDS No: 017-0260) with space group I_{41}/amd (141).[15,32] There were no traces of impurity phases present in the recorded patterns. Here it is interesting to note that both the phosphors were prepared under similar environmental

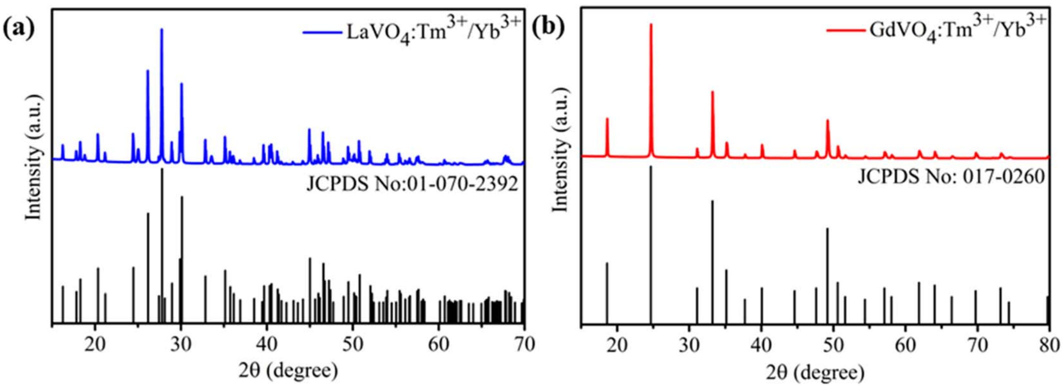

Fig. 1 X-ray diffraction pattern of 0.3 mol% Tm^{3+}/5 mol% Yb^{3+} codoped (a) monazite type $LaVO_4$ (b) zircon type $GdVO_4$ phosphors.

conditions but both have resulted different crystal phases. The $GdVO_4$ sample is in its common crystal phase however, $LaVO_4$ sample is in less common monoclinic phase. The doping position of Tm^{3+}/Yb^{3+} ions in $LaVO_4$ and $GdVO_4$ hosts can be calculated on the basis of percentage radius variance (Δ_r), which can be given by;[33]

$$\Delta_r = \frac{R_h(\mathrm{CN}) - R_d(\mathrm{CN})}{R_h(\mathrm{CN})} \times 100\%$$

where R_h and R_d represents the ionic radii of host and doping ion, respectively. Using above formula, Δ_r (%) for V^{5+} (0.54 Å, CN = 6) with Tm^{3+} (0.88 Å, CN = 6) and Yb^{3+} (0.868 Å, CN = 6) ions are calculated to be 63% and 60.74% respectively. Whereas, Δ_r (%) for La^{3+} (1.032 Å, CN = 6) with Tm^{3+} (0.88 Å, CN = 6) and Yb^{3+} (0.868 Å, CN = 6) pairs are estimated to be 14.72% and 15.89% respectively. It is widely assumed that preferred replacement requires a radius variance (Δ_r) of about 15% between the dopant and host ions. So, this calculation favours the substitution of La^{3+} with Tm^{3+}/Yb^{3+} ions. Similarly, for $GdVO_4$: Tm^{3+}/Yb^{3+} phosphor the Δ_r (%) for Gd^{3+} (0.935 Å, CN = 6) with Tm^{3+} (0.88 Å, CN = 6) and Yb^{3+} (0.868 Å, CN = 6) ions comes out to be 5.88% and 7.16%, respectively which favours the substitution of Gd^{3+} ion with Tm^{3+}/Yb^{3+} pairs.

3.2. UV-vis-NIR absorption spectroscopy

Fig. 2(a) depicts the UV-vis-NIR absorption spectra of 0.3 mol% Tm^{3+}/5 mol% Yb^{3+}: $LaVO_4$ and 0.3 mol%Tm^{3+}/5 mol% Yb^{3+}: $GdVO_4$ phosphors recorded in diffuse reflectance mode in the 200–1200 nm wavelength range. The spectra of both the phosphors show broad absorption bands between 200 and 400 nm, with two peaks centred at 260 and 305 nm. These peaks are arising due to charge transfer state (CTS) transitions from O^{2-} to V^{+5} ions.[34,35]. Apart from these bands, both the spectra contain three absorption peaks due to 4f–4f transition of Tm^{3+} and Yb^{3+} ions. The band centred at 695 and 797 nm are attributed to $^3F_3 \leftarrow {}^3H_6$ and $^3H_4 \leftarrow {}^3H_6$ transitions of Tm^{3+} ion while the broad absorption band at 976 nm is present due to $^2F_{5/2} \leftarrow {}^2F_{7/2}$ transition of Yb^{3+} ion.[36]

The above absorption spectra are further used to calculate the optical band gap of the samples. With the use of Wood–Tauc (W–T) formula and the Kubelka–Munk (K–M) function, the band gap of phosphor materials may be determined. The (W–T) formula for bandgap energy E_g is given by[37]

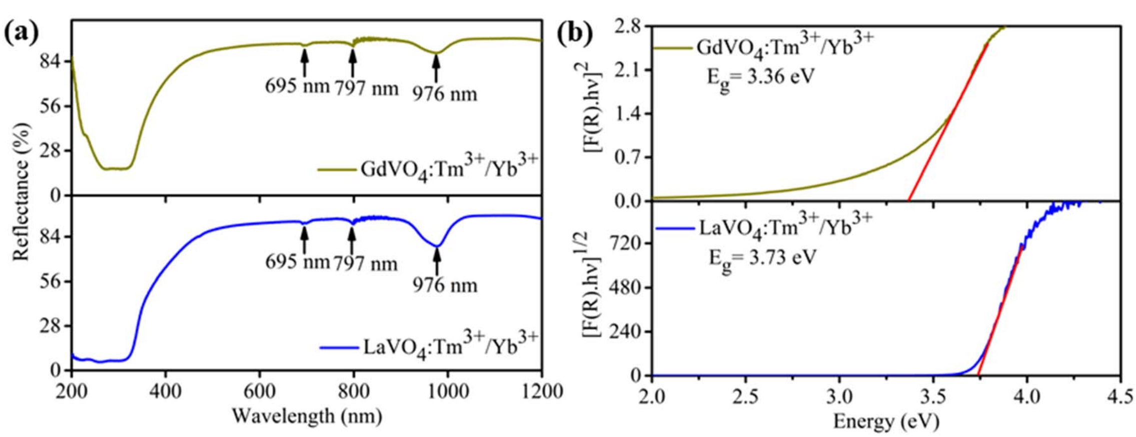

Fig. 2 (a) UV-vis-NIR absorption spectra in diffuse reflectance mode of Tm^{3+}/Yb^{3+} codoped monazite type $LaVO_4$ and zircon type $GdVO_4$ phosphors; (b) Kubelka–Munk plots to estimate the optical band gap energies of the synthesized phosphors.

$$\alpha = \frac{A(h\nu - E_g)^n}{h\nu} \tag{1}$$

where α is the linear absorption coefficient of the material, E_g, $h\nu$ and A are the optical bandgap energy, incident photon energy and A is the proportionality constant, respectively. The K–M function is defined as[38]

$$F(R) = \frac{K}{S} = \frac{(1-R)^2}{2R} \tag{2}$$

where K, S and R are the absorption coefficient, scattering factor and $R = R_{sample}/R_{standard}$ known as reflectance of material, respectively. The optical band gap energy is estimated by combining eqn (1) and (2) which is given by;

$$[F(R)h\nu] = B(h\nu - E_g)^n \tag{3}$$

where B is a constant called the band tailoring parameter and n is a constant that represents the nature of band transition and can have values 1/2, 2, 3/2 or 3 for allowed direct, allowed indirect, forbidden direct and forbidden indirect transitions, respectively. Previous reports indicate that monazite type $LaVO_4$ is an indirect band gap material while tetragonal $GdVO_4$ is a direct band gap material.[15,35,39,40] For estimation of band gap values, the plots of $[F(R)h\nu]^{1/n}$ *versus* $h\nu$ for indirect and direct band gap transitions are shown in Fig. 2(b). From the graph, the value of E_g is extracted by extrapolating the linear fitted regions to $[F(R)h\nu]^{1/n} = 0$. By this way, band gap for Tm^{3+}/Yb^{3+} codoped monazite type $LaVO_4$ is determined to be 3.73 eV, and that of Tm^{3+}/Yb^{3+} codoped zircon type $GdVO_4$ is estimated to be 3.36 eV. Both the calculated band gap values are in consistent with the reported results.

3.3. Upconversion emission and energy level diagram

Fig. 3(a) compares the UC emission spectra of 0.3 mol% Tm^{3+}/5 mol% Yb^{3+}: $LaVO_4$ and 0.3 mol% Tm^{3+}/5 mol% Yb^{3+}: $GdVO_4$ phosphors at 66 mW excitation power of 980 nm laser diode. In both the phosphors, three emission bands are observed at 475, 647 and 700 nm wavelengths. These bands are attributed to the $^1G_4 \rightarrow {}^3H_6$, $^1G_4 \rightarrow {}^3F_4$ and $^3F_3 \rightarrow {}^3H_6$ transitions of Tm^{3+} ion, respectively. It is interesting to see that UC emission intensity of $GdVO_4$ phosphor is around 24 times higher than the $LaVO_4$ phosphor, although both samples were synthesized under similar conditions and contain same concentrations of the dopant ions. Moreover, it was expected that monoclinic phase should show higher emission compared to the tetragonal phase due to lower symmetry in monoclinic phase. The blue emission (475 nm) is found to dominant over red bands (647, 700 nm) in both the phosphors. The inset of Fig. 3(a) shows the enlarged view of the spectra in wavelength range 600–730 nm for better visibility of weak emission bands.

To better understand the observed UC emission bands in both the phosphors, energy level diagram is illustrated in Fig. 3(b). The Yb^{3+} ion works as sensitizer for this system as it has higher absorption cross-section for 980 nm excitation. After absorbing 980 nm photon energy Yb^{3+} ions excite to $^2F_{5/2}$ level and then transfer the photon energy to nearby Tm^{3+} ion *via* various UC processes. After getting energy from Yb^{3+} through ET(1) process, ground state ($^3H_6$) Tm^{3+} ions are raised to excited state $^3H_5$ followed by non-radiative decay to $^3F_4$ level, while Yb^{3+} ion goes back to its ground state $^2F_{7/2}$. The Tm^{3+} ions in $^3F_4$ level again uplifted to $^3F_2$ excited state by absorbing next 980 nm photon energy transferred *via* ET(2) process of Yb^{3+} ion. Tm^{3+} ions while coming back to $^3H_4$ level non-radiatively, a part of them makes radiative transition from $^3F_3$ to $^3H_6$ by emitting red light of wavelength of 700 nm. Since Yb^{3+} ions continuously transfer their absorbed energy to Tm^{3+} ions resulting transition of Tm^{3+} ions from $^3H_4$ to $^1G_4$ level *via* ET (3) process. Some part of Tm^{3+} ions in $^1G_4$ level make radiative emission to $^3H_6$ ground state by emitting blue light at 475 nm while rest part of Tm^{3+} population in $^1G_4$ state goes radiatively to $^3F_4$ state *via* emission of 647 nm wavelength. It can be seen that 475 nm and 647 nm UC emission belongs to three photon absorption processes while 700 nm emission is due to two photon process.

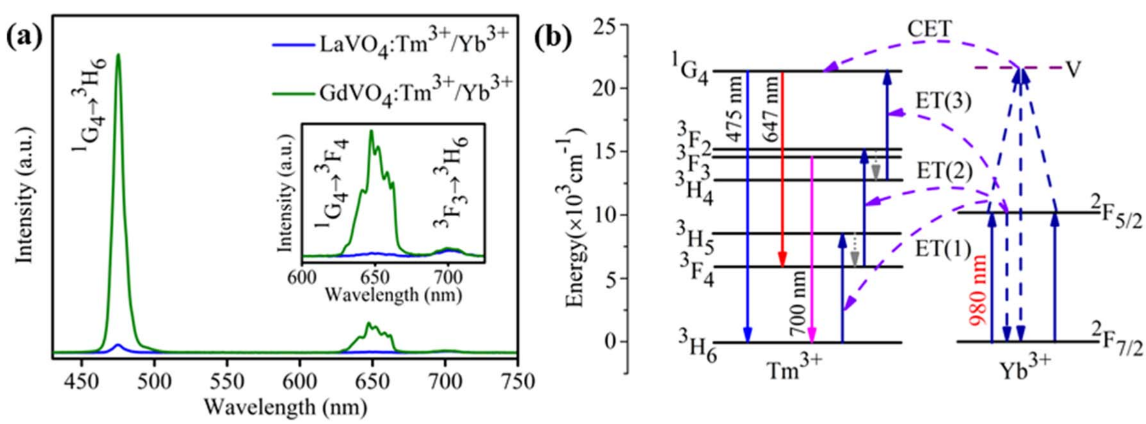

Fig. 3 (a) Comparison of upconversion emission spectra of 0.3 mol% Tm^{3+}/5 mol% Yb^{3+} codoped $LaVO_4$ and $GdVO_4$ phosphors under 980 nm laser diode excitation; inset shows the enlarged spectra in 600–730 nm range; (b) energy level diagram of Tm^{3+} and Yb^{3+} ions with possible upconversion processes in both the hosts.

3.4. Pump power dependence study

Fig. 4(a and b) shows the UC emission spectra of $LaVO_4$ and $GdVO_4$ based phosphors at various pump powers of 980 nm laser diode, respectively. The UC emission in both the samples increases upon increasing pump power from 30 to 104 mW. Interestingly, the red emission (700 nm) is found to increase rapidly in $LaVO_4$ sample than the $GdVO_4$. For an unsaturated UC process, emission intensity is related to the pump power as;[41]

$$I \propto P^n \tag{4}$$

where I and P are the UC emission intensity and excitation pump power. 'n' is the number of NIR photons engaged in populating the emitting levels. Inset of Fig. 4(a and b) shows the ln–ln plot of UC emission intensity *versus* pump power for $^1G_4 \rightarrow {}^3H_6$ (475 nm) and $^3F_3 \rightarrow {}^3H_6$ (700 nm) transitions. It is found that for 475 and 700 nm emissions, the slopes are 1.19 and 1.57, respectively for $LaVO_4$ sample whereas slopes of 1.51 and 1.42 respectively are found in $GdVO_4$ sample. These values are presenting two photon processes for 475 and 700 nm emissions. However, the slope values for 700 nm in both the samples are in good agreement with two photon process as proposed by energy level diagram (Fig. 3(b)). But the observed slope values for 475 nm are less than expected value of ~3. This may be due to the fact that the cooperative energy transfer (CET) process also takes part in UC emission. As represented in energy level diagram, $^1G_4$ level of Tm^{3+} ion is populated from a virtual state (V) where two excited Yb^{3+} ion simultaneously transferred their energy. In this case, only 2 excitation photons are required to emit 475 nm photons. Hence, the slope values for 475 nm emission in both the systems are deviated from expected value of ~3. Such kind of observations for Tm^{3+}/Yb^{3+} doped systems are also reported by various researchers.[26,41,42]

3.5. Optical thermometry

To explore the possibility of synthesized 0.3 mol% Tm^{3+}/5 mol% Yb^{3+}: $LaVO_4$ and 0.3 mol% Tm^{3+}/5 mol% Yb^{3+}: $GdVO_4$ phosphors for optical temperature sensing, the temperature dependent UC spectra were recorded in the temperature range 300–653 K upon 980 nm laser diode excitation, as shown in Fig. 5(a and b). The laser pump power was kept at minimum (~66 mW) to avoid laser induced heating of the sample. It can be seen that UC emission intensity of 475 nm ($^1G_4 \rightarrow {}^3H_6$) and 647 nm ($^1G_4 \rightarrow {}^3F_4$) bands decreases with increasing temperature, while 700 nm ($^3F_3 \rightarrow {}^3H_6$) emission intensity increases with increasing temperature in both the samples. Since, $^3F_3$ and $^3H_4$ levels are the thermally coupled levels with energy gap of ~1817 cm^{-1} (ref. 25) and hence thermal excitation increases the population of $^3F_3$ from $^3H_4$ level with enhancement of 700 nm band at elevated temperatures. Here authors have plotted the intensity ratio of red/blue bands (I_{700}/I_{475}) for both the phosphors against temperature and pump power. For the plot shown in Fig. 5(c and d) the intensity ratio (I_{700}/I_{475}) is found to increase faster for $LaVO_4$ sample than the $GdVO_4$ sample. Due to different intensity response of emission bands with temperature, the non-thermally coupled levels $^3F_3$ and $^1G_4$ (700 and 475 nm) of both the samples were utilized for fluorescence intensity ratio (FIR) based optical thermometry.

For non-thermally coupled levels (NTCLs), the FIR data can be well fitted through following exponential equation;[27,30,43]

$$\mathrm{FIR} = \frac{I_{700}}{I_{475}} = A\exp\left(-\frac{B}{T}\right) + C \tag{5}$$

where A, B and C are constants whose values can be found by fitting the experimental data. T denotes the absolute temperature. As illustrated in Fig. 6(a and b), the best fits of FIR to temperature are FIR = 75.03 × exp(−1860.44/T) + 0.26 and FIR = 1062.55 × exp(−4403.45/T) + 0.07 for $LaVO_4$: Tm^{3+}/Yb^{3+} and $GdVO_4$: Tm^{3+}/Yb^{3+} samples, respectively. The absolute sensitivity (S_a) is defined as the rate of change of FIR with temperature and expressed as;[43]

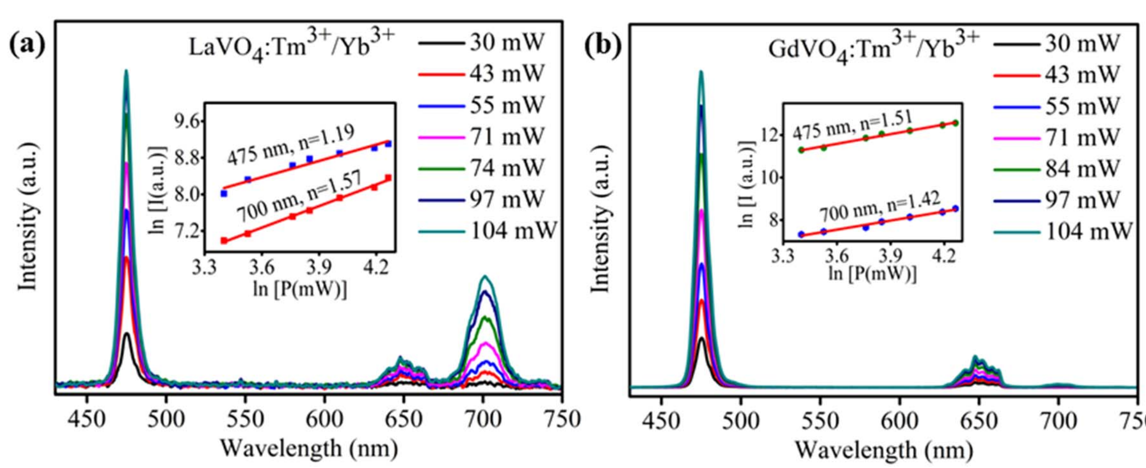

Fig. 4 Pump power dependent UC spectra of Tm^{3+}/Yb^{3+} codoped (a) $LaVO_4$ (b) $GdVO_4$ phosphors. Inset of both figures represent the ln–ln plot of UC emission intensity *versus* excitation power.

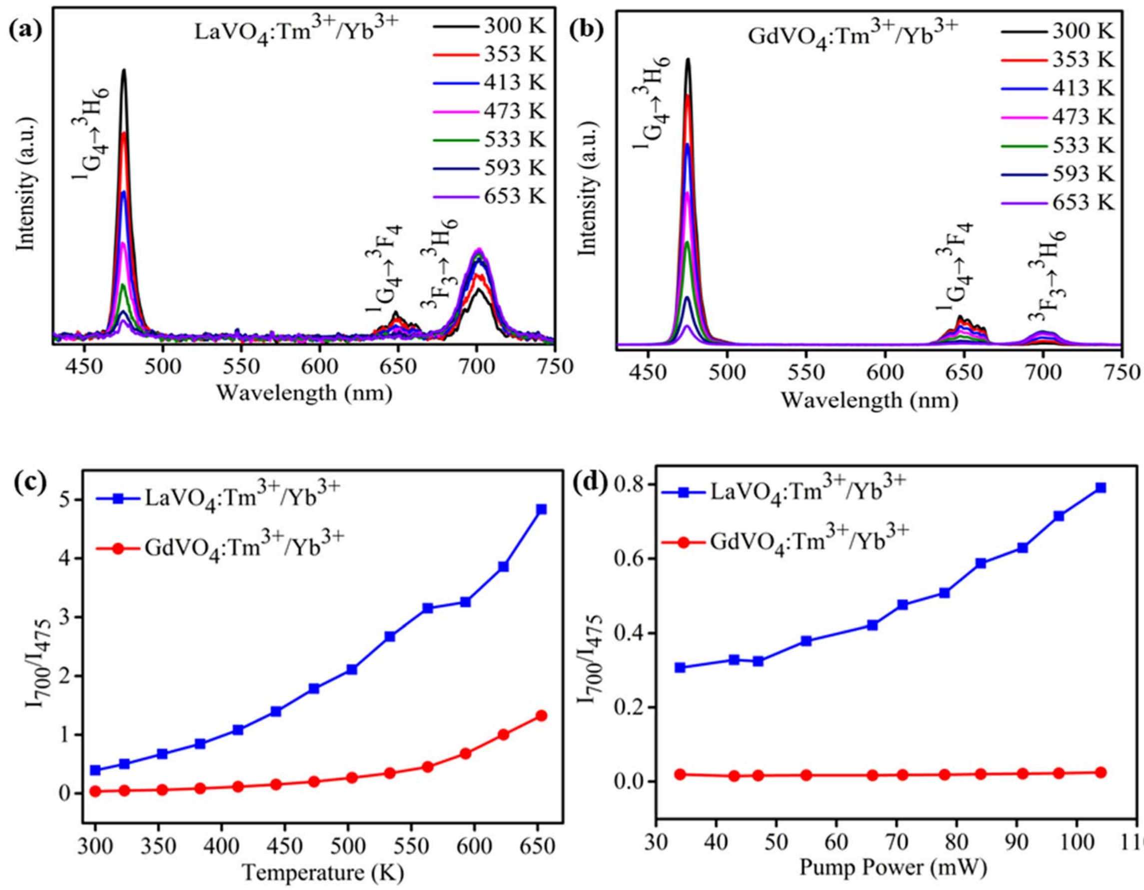

Fig. 5 (a) Temperature dependent UC spectra upon 980 nm laser excitation in temperature range 300–653 K of (a) Tm^{3+}/Yb^{3+}: $LaVO_4$ (b) Tm^{3+}/Yb^{3+}: $GdVO_4$ phosphors. Variation in the ratio of red/blue emission band (I_{700}/I_{475}) in both the phosphors at varying (c) temperature (d) pump power.

$$S_a = \frac{d(FIR)}{dT} = \frac{AB}{T^2}\exp\left(-\frac{B}{T}\right) \tag{6}$$

Fig. 6(c and d) shows the plot of absolute sensitivity as a function of temperature for both the samples. It is observed that the sensitivity increases from room temperature to studied (653 K) temperature. The maximum sensitivity for $LaVO_4$: Tm^{3+}/Yb^{3+} phosphor is found to be 19.0×10^{-3} K^{-1} at 653 K (Fig. 6(c)) whereas, maximum sensitivity for $GdVO_4$: Tm^{3+}/Yb^{3+} phosphor is found to 13.0×10^{-3} K^{-1} at 653 K (Fig. 6(d)). However, it seems that sensitivity of $GdVO_4$ will increase above 653 K. The observed value is compared with Tm^{3+}/Yb^{3+} codoped samples in which TCLs are utilized for temperature sensing measurement as given in Table 1.

Some authors have also fitted FIR data of NTCLs with help of polynomial equation.[44,45] So, to examine the difference between both the fittings, we have fitted the same FIR data with the polynomial equation as given below;

$$FIR = \frac{I_{700}}{I_{475}} = A + BT + CT^2 + DT^3 \tag{7}$$

where *A*, *B*, *C* and *D* are the constants. As shown in Fig. 7(a and b) the FIR *versus* temperature data can be well fitted by above polynomial equation. The best fit of FIR to temperature for $LaVO_4$: Tm^{3+}/Yb^{3+} is FIR= $(2.34 \times 10^{-3}) - (1.01 \times 10^{-3})T + (3.22 \times 10^{-6})T^2 + (1.41 \times 10^{-8})T^3$ and for $GdVO_4$: Tm^{3+}/Yb^{3+} is FIR = $(-3.75) + (0.02)T - (7.21 \times 10^{-5})T^2 + (6.14 \times 10^{-8})T^3$. The absolute sensitivity using eqn (7)can be written as,

$$S_a = \frac{d(FIR)}{dT} = B + 2CT + 3DT^2 \tag{8}$$

The calculated sensitivity as a function of temperature is shown in Fig. 7(c and d) for both the samples. The maximum absolute sensitivity for $LaVO_4$: Tm^{3+}/Yb^{3+} phosphor is found to be 21.2×10^{-3} K^{-1} at 653 K (Fig. 7(c)) whereas, absolute sensitivity for $GdVO_4$: Tm^{3+}/Yb^{3+} phosphor is calculated to be 13.0×10^{-3} K^{-1} at 653 K (Fig. 7(d)). Only slight variation in sensitivity is seen for both the fittings and it can be concluded that both the techniques are equally well.

3.6. CIE chromaticity diagram

Colour coordinates study of prepared phosphors at various temperatures was done in the temperature range of 300–653 K

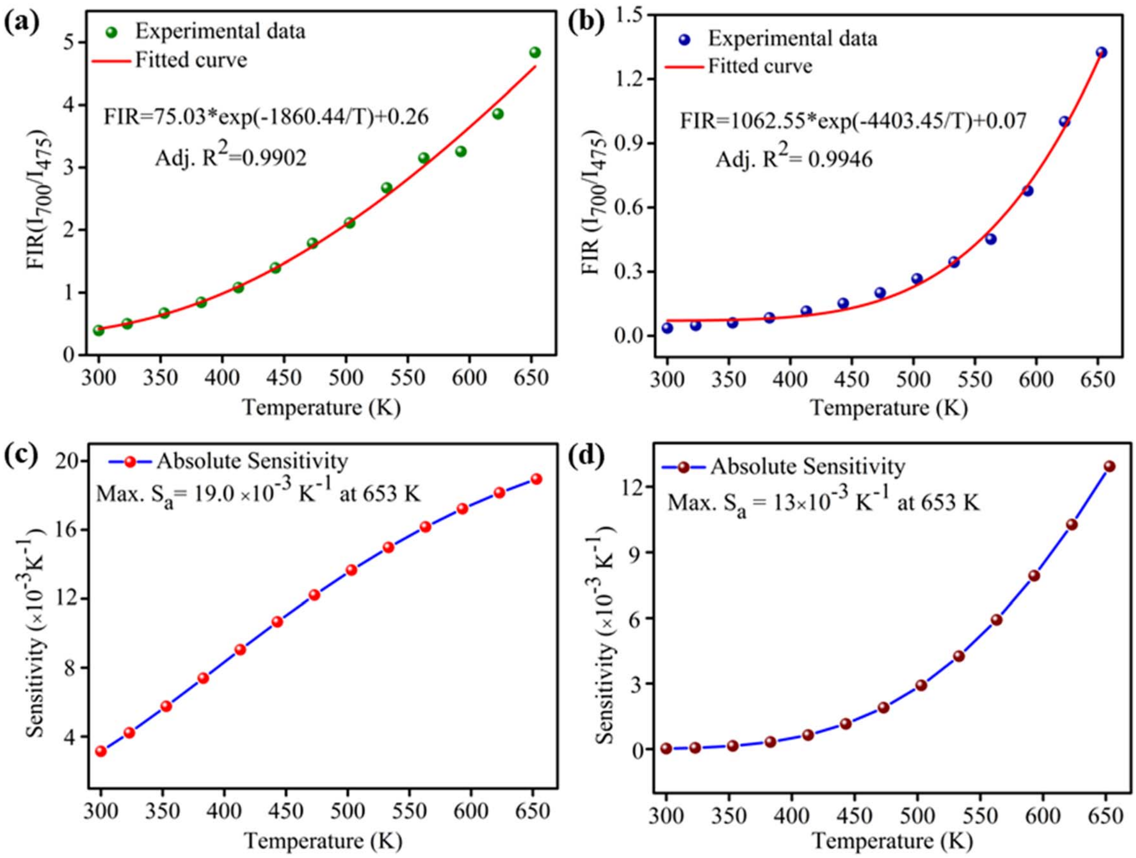

Fig. 6 Exponential fitting of FIR data of non-thermally coupled levels ($^3F_3$ and $^1G_4$) as a function of temperature for (a) Tm^{3+}/Yb^{3+}: $LaVO_4$ (b) Tm^{3+}/Yb^{3+}: $GdVO_4$ phosphors; absolute sensitivity as a function of temperature for (c) Tm^{3+}/Yb^{3+}: $LaVO_4$ (d) Tm^{3+}/Yb^{3+}: $GdVO_4$ phosphors.

Table 1 Comparison of absolute sensitivity of Tm^{3+} doped luminescent materials

Samples	Transitions	Temperature range (K)	$S_{a\text{-}max}$ ($\times 10^{-3}$ K^{-1})	Ref.
$LaVO_4$: Tm^{3+}/Yb^{3+} (exponential fitting)	$^3F_3 \rightarrow {}^3H_6$ $^1G_4 \rightarrow {}^3H_6$	300–653	19.00 (653 K)	This work
$LaVO_4$: Tm^{3+}/Yb^{3+} (polynomial fitting)	$^3F_3 \rightarrow {}^3H_6$ $^1G_4 \rightarrow {}^3H_6$	300–653	21.20 (653 K)	This work
$GdVO_4$: Tm^{3+}/Yb^{3+} (exponential fitting)	$^3F_3 \rightarrow {}^3H_6$ $^1G_4 \rightarrow {}^3H_6$	300–653	13.00 (653 K)	This work
$GdVO_4$: Tm^{3+}/Yb^{3+} (polynomial fitting)	$^3F_3 \rightarrow {}^3H_6$ $^1G_4 \rightarrow {}^3H_6$	300–653	13.00 (653 K)	This work
$Bi_7F_{11}O_5$: Tm^{3+}/Yb^{3+}	$^3F_3 \rightarrow {}^3H_6$ $^3H_4 \rightarrow {}^3H_6$	303–573	14.00 (303 K)	46
$SrWO_4$: Tm^{3+}/Yb^{3+}	$^3F_3 \rightarrow {}^3H_6$ $^3H_4 \rightarrow {}^3H_6$	308–573	6.17 (323 K)	5
$BaGd_2ZnO_5$: Tm^{3+}/Yb^{3+}	$^1G_{4(1)} \rightarrow {}^3H_6$ $^1G_{4(2)} \rightarrow {}^3H_6$	313–573	5.50 (323 K)	47
$Na_2Y_2B_2O_7$: Tm^{3+}/Yb^{3+}	$^1G_{4(i)} \rightarrow {}^3H_6$ $^1G_{4(j)} \rightarrow {}^3H_6$	300–623	4.54 (300 K)	48
Y_2O_3: Tm^{3+}/Yb^{3+}	$^1G_{4(a)} \rightarrow {}^3H_6$ $^1G_{4(b)} \rightarrow {}^3H_6$	303–753	3.50 (303K)	26
$ZnWO_4$: $Tm^{3+}/Yb^{3+}/Mg^{2+}$	$^1G_{4(1)} \rightarrow {}^3H_6$ $^1G_{4(2)} \rightarrow {}^3H_6$	300–600	3.40 (300 K)	49
Y_2O_3: $Tm^{3+}/Yb^{3+}/Gd^{3+}$	$^1G_{4(a)} \rightarrow {}^3H_6$ $^1G_{4(b)} \rightarrow {}^3H_6$	298–533	1.33 (298 K)	20
CaZnOS: Tm^{3+}/Yb^{3+}	$^1G_{4(a)} \rightarrow {}^3H_6$ $^1G_{4(b)} \rightarrow {}^3H_6$	303–423	1.00 (303 K)	44

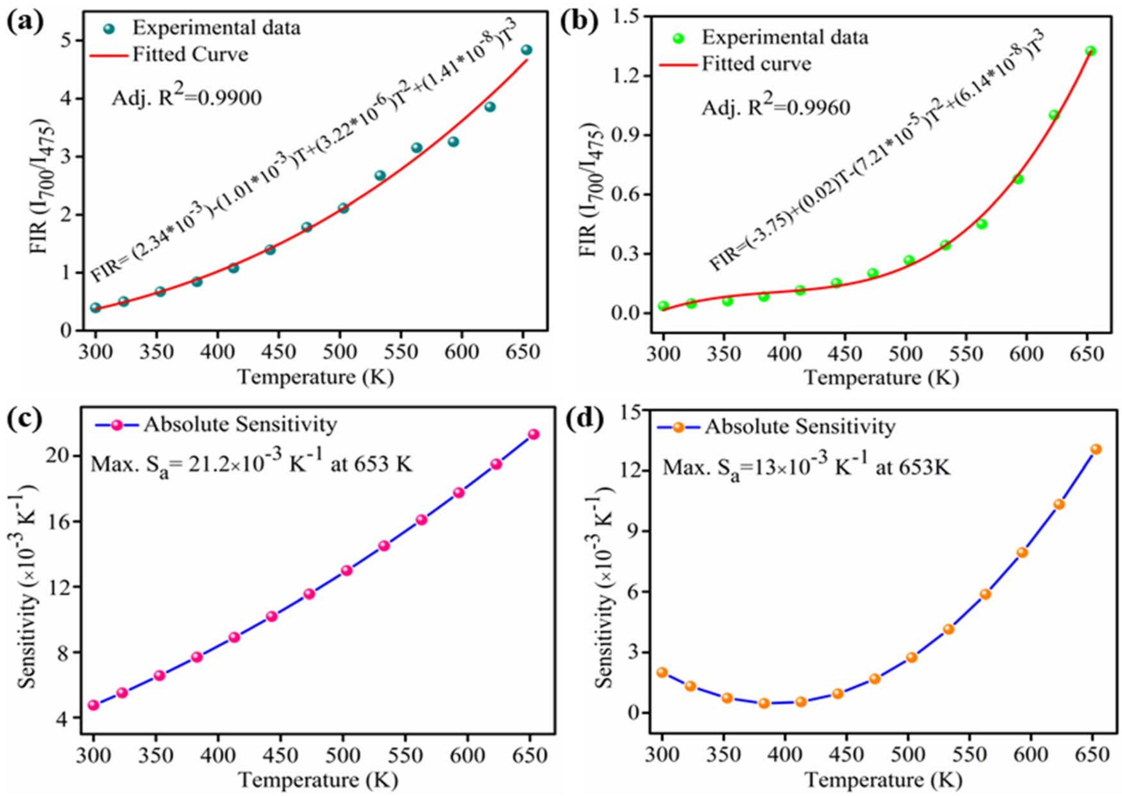

Fig. 7 Polynomial fitting of FIR data of NTCLs ($^3F_3$ and $^1G_4$) as a function of temperature for (a) Tm^{3+}/Yb^{3+}: $LaVO_4$ (b) Tm^{3+}/Yb^{3+}: $GdVO_4$ phosphors; absolute sensitivity as a function of temperature for (c) Tm^{3+}/Yb^{3+}: $LaVO_4$ (d) Tm^{3+}/Yb^{3+}: $GdVO_4$ phosphors.

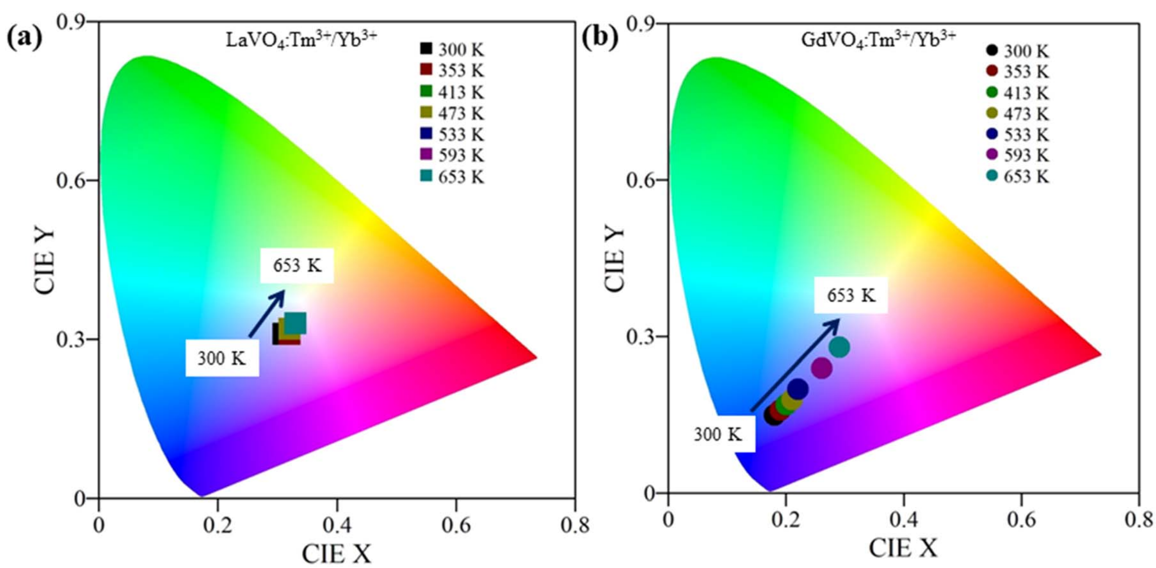

Fig. 8 CIE colour chromaticity diagram of (a) $LaVO_4$: 0.3 mol% Tm^{3+}/5 mol% Yb^{3+} (b) $GdVO_4$: 0.3 mol% Tm^{3+}/5 mol% Yb^{3+} phosphors. Colour change is more prominent is $GdVO_4$ phosphor.

under 980 nm laser excitation at fixed pump power of 66 mW. The coordinates are shown in CIE plot in Fig. 8(a and b). The colour tuning behaviour is prominent in $GdVO_4$ phosphor. Coordinates of $LaVO_4$: Tm^{3+}/Yb^{3+} phosphor are only slightly shifted from light blue (0.31, 0.31) to pure white (0.33, 0.33) with increasing temperature as shown in Fig. 8(a). On other hand, $GdVO_4$: Tm^{3+}/Yb^{3+} phosphor shows deep blue colour (0.18, 0.15) at 300 K and approaches nearly white light (0.29, 0.28) at 653 K, shown in Fig. 8(b).

4. Conclusions

The $LaVO_4$: Tm^{3+}/Yb^{3+} and $GdVO_4$: Tm^{3+}/Yb^{3+} upconversion phosphors were successfully synthesized using solid state reaction method. The $LaVO_4$ sample is found in monoclinic crystal phase while $GdVO_4$ is found in tetragonal crystal phase. Upon 980 nm laser diode excitation the $GdVO_4$: Tm^{3+}/Yb^{3+} has resulted several fold intense blue upconversion emission than the $LaVO_4$: Tm^{3+}/Yb^{3+} phosphor. The non-thermally coupled levels *viz.* $^3F_3$ (700 nm) and $^1G_4$ (475 nm) were utilized for optical thermometry in both the phosphors and two different functions were used for fitting the FIR *versus* temperature data. For $LaVO_4$: Tm^{3+}/Yb^{3+} phosphor, exponential fitting gives a maximum absolute sensitivity of 19.0×10^{-3} K^{-1} at 653 K while polynomial fitting provides a maximum value of 21.2×10^{-3} K^{-1} at 653 K. Similarly, for $GdVO_4$: Tm^{3+}/Yb^{3+} phosphor, maximum absolute sensitivity of 13.0×10^{-3} K^{-1} at 653 K is observed using the both kind of fitting functions. It is concluded that $LaVO_4$: Tm^{3+}/Yb^{3+} phosphor provides higher sensing sensitivity compared to $GdVO_4$: Tm^{3+}/Yb^{3+} phosphor.

Conflicts of interest

There are no conflicts to declare.

Acknowledgements

Madan M. Upadhyay is thankful to IIT(ISM) Dhanbad for providing financial support in terms of Senior Research Fellowship (SRF). Authors also acknowledge DST-SERB, New Delhi India (Project no: EMR/000228/2017) for the lab facilities.

References

1 Y. Du, Y. Wang, Z. Deng, X. Chen, X. Yang, T. Sun, X. Zhang, G. Zhu, S. F. Yu and F. Wang, *Adv. Opt. Mater.*, 2020, **8**, 1900968.
2 P. Ramasamy, P. Manivasakan and J. Kim, *RSC Adv.*, 2014, **4**, 34873–34895.
3 Y. Zhong, I. Rostami, Z. Wang, H. Dai and Z. Hu, *Adv. Mater.*, 2015, **27**, 6418–6422.
4 A. Chen, H. Gong, R. Wei, H. Guo and F. Hu, *J. Alloys Compd.*, 2022, **921**, 166094.
5 H. Song, C. Wang, Q. Han, X. Tang, W. Yan, Y. Chen, J. Jiang and T. Liu, *Sens. Actuators, A*, 2018, **271**, 278–282.
6 Y. Li, J. Yang, M. Wang, Y. Zhu, H. Zhu, D. Yan, C. Liu, C. Xu and Y. Liu, *J. Lumin.*, 2022, 118935.
7 X. Wu, G. Chen, J. Shen, Z. Li, Y. Zhang and G. Han, *Bioconjug. Chem.*, 2015, **26**, 166–175.
8 M. V. DaCosta, S. Doughan, Y. Han and U. J. Krull, *Anal. Chim. Acta*, 2014, **832**, 1–33.
9 Q. Cheng, J. Sui and W. Cai, *Nanoscale*, 2012, **4**, 779–784.
10 S. Sinha, M. K. Mahata and K. Kumar, *New J. Chem.*, 2019, **43**, 5960–5971.
11 K. Du, X. Xu, S. Yao, P. Lei, L. Dong, M. Zhang, J. Feng and H. Zhang, *CrystEngComm*, 2018, **20**, 1945–1953.
12 G. Chen, H. Qiu, P. N. Prasad and X. Chen, *Chem. Rev.*, 2014, **114**, 5161–5214.
13 V. Tamilmani, A. Kumari, V. K. Rai, B. Unni Nair and K. J. Sreeram, *J. Phys. Chem. C*, 2017, **121**, 4505–4516.
14 F. Zhang, G. Li, W. Zhang and Y. L. Yan, *Inorg. Chem.*, 2015, **54**, 7325–7334.
15 M. Michalska, J. B. Jasiński, J. Pavlovsky, P. Żurek-Siworska, A. Sikora, P. Gołębiewski, A. Szysiak, V. Matejka and J. Seidlerova, *J. Lumin.*, 2021, **233**, 117934.
16 W. Yin, L. Zhou, Z. Gu, G. Tian, S. Jin, L. Yan, X. Liu, G. Xing, W. Ren, F. Liu, Z. Pan and Y. Zhao, *J. Mater. Chem.*, 2012, **22**, 6974.
17 B. Shao, Q. Zhao, N. Guo, Y. Jia, W. Lv, M. Jiao, W. Lü and H. You, *CrystEngComm*, 2014, **16**, 152–158.
18 Y. Oka, T. Yao and N. Yamamoto, *J. Solid State Chem.*, 2000, **152**, 486–491.
19 C.-J. Jia, L.-D. Sun, L.-P. You, X.-C. Jiang, F. Luo, Y.-C. Pang and C.-H. Yan, *J. Phys. Chem. B*, 2005, **109**, 3284–3290.
20 M. M. Upadhyay and K. Kumar, *J. Rare Earths*, 2022, DOI: 10.1016/j.jre.2022.07.005.
21 S. K. Gupta, M. Abdou, J. P. Zuniga, P. S. Ghosh and Y. Mao, *J. Lumin.*, 2020, **224**, 117312.
22 P. Tadge, I. R. Martín, S. B. Rai, S. Sapra, T. M. Chen, V. Lavín, R. S. Yadav and S. Ray, *J. Lumin.*, 2022, **252**, 119261.
23 M. I. Sarkar, N. K. Mishra and K. Kumar, *Methods Appl. Fluoresc.*, 2023, **11**, 014002.
24 N. Kumar Mishra, M. M. Upadhyay, S. Kumar and K. Kumar, *Spectrochim. Acta, Part A*, 2022, **282**, 121664.
25 Y. Zhuang, D. Wang and Z. Yang, *Opt. Mater.*, 2022, **126**, 112167.
26 D. Li, Y. Wang, X. Zhang, K. Yang, L. Liu and Y. Song, *Opt. Commun.*, 2012, **285**, 1925–1928.
27 X. Tu, J. Xu, M. Li, T. Xie, R. Lei, H. Wang and S. Xu, *Mater. Res. Bull.*, 2019, **112**, 77–83.
28 H. Zhou, N. An, K. Zhu, J. Qiu, L. Yue, L.-G. Wang and L. Ye, *J. Lumin.*, 2021, **229**, 117656.
29 W. Ge, M. Xu, J. Shi, J. Zhu and Y. Li, *Chem. Eng. J.*, 2020, **391**, 123546.
30 H. Lv, P. Du, W. Li and L. Luo, *ACS Sustainable Chem. Eng.*, 2022, **10**, 2450–2460.
31 K. Shwetabh, M. M. Upadhyay and K. Kumar, *RSC Adv.*, 2023, **13**, 9377–9386.
32 J. H. Oh, B. K. Moon, B. C. Choi, J. H. Jeong, J. H. Kim and H. S. Lee, *Solid State Sci.*, 2015, **42**, 1–5.
33 I. Gupta, D. Singh, S. Singh, P. Kumar, S. Bhagwan and V. Kumar, *Chem. Phys. Lett.*, 2023, **814**, 140350.
34 E. Rai, R. S. Yadav, D. Kumar, A. K. Singh, V. J. Fulari and S. B. Rai, *J. Lumin.*, 2022, **241**, 118519.
35 D. J. Jovanović, T. V. Gavrilović, S. D. Dolić, M. Marinović-Cincović, K. Smits and M. D. Dramićanin, *Opt. Mater.*, 2018, **82**, 1–6.
36 R. S. Yadav, S. J. Dhoble and S. B. Rai, *Sens. Actuators, B*, 2018, **273**, 1425–1434.
37 A. Dwivedi, K. Mishra and S. B. Rai, *J. Phys. D. Appl. Phys.*, 2015, **48**, 435103.
38 S. Sinha, M. K. Mahata, H. C. Swart, A. Kumar and K. Kumar, *New J. Chem.*, 2017, **41**, 5362–5372.

39 L. Sun, X. Zhao, Y. Li, P. Li, H. Sun, X. Cheng and W. Fan, *J. Appl. Phys.*, 2010, **108**, 093519.
40 L. Yang, L. Li, M. Zhao and G. Li, *Phys. Chem. Chem. Phys.*, 2012, **14**, 9956.
41 X. Tu, J. Xu, M. Li, T. Xie, R. Lei, H. Wang and S. Xu, *Mater. Res. Bull.*, 2019, **112**, 77–83.
42 G. Chen, R. Lei, H. Wang, F. Huang, S. Zhao and S. Xu, *Opt. Mater.*, 2018, **77**, 233–239.
43 D. Chen, S. Liu, Z. Wan and Y. Chen, *J. Alloys Compd.*, 2016, **672**, 380–385.
44 W. Gao, W. Ge, J. Shi, X. Chen and Y. Li, *J. Solid State Chem.*, 2021, **297**, 122063.
45 M. Vega, I. R. Martin, E. Cortés-Adasme and J. Llanos, *J. Lumin.*, 2022, **244**, 118687.
46 T. Wang, Y. Li, T. Liu, Y. Peng, Z. Yin, Z. Yang, J. Qiu and Z. Song, *J. Lumin.*, 2020, **221**, 117034.
47 Z. Sun, G. Liu, Z. Fu, X. Zhang, Z. Wu and Y. Wei, *Curr. Appl. Phys.*, 2017, **17**, 255–261.
48 A. K. Soni, R. Dey and V. K. Rai, *RSC Adv.*, 2015, **5**, 34999–35009.
49 R. S. Yadav, S. J. Dhoble and S. B. Rai, *Sens. Actuators, B*, 2018, **273**, 1425–1434.